The structural basis for peptide selection by the transport receptor OppA

Berntsson, Ronnie P-A; Doeven, Mark K.; Fusetti, Fabrizia; Duurkens, Ria H.; Sengupta, Durba; Marrink, Siewert-Jan; Thunnissen, Andy-Mark W. H.; Poolman, Bert; Slotboom, Dirk-Jan

Published in:
EMBO Journal

DOI:
10.1038/emboj.2009.65

Publication date:
2009

Supplementary information

Oligomeric state of OppA*

Crystal structures of substrate-binding proteins (SBPs) have shown that they are monomers with one substrate-binding site per molecule (Quiocho & Ledvina, 1996). However, recently it was shown that TakP, a SBP from a tripartite ATP-independent transporter, is a dimer (Gonin *et al*, 2007). Moreover, in ATP-binding cassette (ABC) transporters containing multiple substrate-binding domains (SBDs) fused to the translocator, co-operativity between these domains has been observed (Biemans-Oldehinkel & Poolman, 2003). Several early experiments also suggested that SBPs self-associate to form dimers or higher order oligomers (Rashed *et al*, 1976; Richarme, 1982; Richarme, 1983) which might be a way to regulate their activity (Antonov *et al*, 1976). To determine the oligomeric state of OppA* we performed light scattering and equilibrium centrifugation measurements.

Sedimentation equilibrium centrifugation (Fig. S1c) and static light scattering experiments (Fig. 1) unambiguously showed that purified OppA* is a monomer. For the ligand-free version of OppA*, the measured molecular weights determined by equilibrium centrifugation and static light scattering were 68.2 kDa and 65.0 kDa, respectively. These values were close to the calculated molecular weight for the monomer of 65.1 kDa, based on the amino acid sequence. Addition of the high-affinity ligand bradykinin did not significantly change the molecular weight determined by sedimentation equilibrium centrifugation. Also, the molecular weight of OppA* with endogenous ligand bound, determined by light scattering, did not differ from that of ligand-free OppA* (Fig. 1). In contrast, the hydrodynamic properties of ligand bound and ligand-free OppA* were significantly different, as indicated by sedimentation velocity measurements (Fig. S1a), and by the elution volumes observed in gel filtration experiments. Consistent with the equilibrium centrifugation data, the sedimentation behaviour of OppA* did not change over the concentration range tested (0.02 to 1.30 mg/mL), indicating that the protein was present as a single-species not undergoing reversible self-association. The average sedimentation coefficient ($s_{20,w}$), however, increased from 4.2 ± 0.1 S in the absence of ligand to 4.6 ± 0.2 S upon the addition of a saturating amount of bradykinin (Fig.

S1b). Moreover, in gel filtration chromatography experiments, ligand-bound OppA* migrated more slowly on a size-exclusion column compared to ligand-free OppA* (Fig. 1). This hydrodynamic behavior thus indicates that ligand-bound OppA* adopts a more compact conformation than the ligand-free protein, consistent with the Venus Flytrap mechanism.

Ligand binding to OppA*

Protein functionality and the removal of endogenous bound substrate were verified by monitoring intrinsic protein fluorescence changes upon titration with peptide (Fig. S4). The K_d and maximum change in fluorescence (F_{max}) were 0.26 μM and 12.3 %, which is close to the values of 0.10 μM and 12.6 % that were obtained previously (Lanfermeijer *et al*, 1999).

Experimental Procedures

Purification of OppA*

Expression of OppA* in *Lactococcus lactis* AMP2/pAMP21 and cell lysis were done as previously described (Lanfermeijer *et al*, 1999), and the soluble fraction was frozen in liquid nitrogen and stored at -80ºC. The lysate was thawed, 0.5 mL Ni^{2+}-sepharose resin (Amersham Biosciences) was added per 50 mL lysate, and the mixture was incubated for 1 h at 4 °C in buffer A (50mM Tris-HCl, 300 mM NaCl, 10% (v/v) glycerol, pH 8.0) supplemented with 15 mM imidazole. Subsequently, the resin was washed with buffer A containing 40 mM imidazole, for 20 column volumes (CV). In case endogenously bound peptides were removed, OppA* was partially unfolded while bound to the resin. The following additional wash steps were performed (all in buffer A with 15 mM imidazol): 40 CV with 2M Guanidine-HCl (GndHCl), 4 CV with 1.5 M GndHCl, 4 CV with 1 M GndHcl, 4 CV with 0.5 M GndHCl and finally 8 CV with 0 M GndHCl. The protein was eluted with 20 mM Na-MES, pH 6.0, 300 mM NaCl, 500 mM imidazole, pH 6.0, 2 CV. For purification of OppA* with endogenously bound peptides, the washing steps with Guanidine-HCl were omitted.
Purified OppA* was concentrated to 0.5 ml in spin concentrators with 30 kDa cut-off (Vivaspin with PES membrane Sartorius), and further purified on a Superdex 200 10/300 GL size exclusion column (Amersham Biosciences) in 20 mM Na-MES, pH 6.0, 150 mM NaCl. Fractions containing OppA were pooled, concentrated 10-fold,

and diluted such that the final buffer composition was 10mM Na-MES, pH 6.0, 10mM NaCl, and finally concentrated again to 11 mg/mL of protein. For co-crystallization with peptides, the peptide (10 mM stock in milliQ water) was mixed 1 to 10 with protein solution yielding final concentrations of 10 mg/mL OppA, 1 mM peptide, 9 mM Na-MES, pH 6.0 and 9 mM NaCl.

Fluorescence titration

Measurements were performed on a Spex Fluorolog 322 fluorescence spectrophotometer (Jobin Yvon) at 25°C in a 1 mL stirred cuvette. For fluorescence titration experiments, 0.5-1 μM bradykinin stock solutions were used, and solutions of bradykinin were added in 1 μL steps. The excitation and emission wavelengths were 280 and 318, respectively, with slit widths of 1 and 2 nm, respectively. Titrations with water in the absence of protein were performed as reference.

Analytical ultracentrifugation

Analytical ultracentrifugation experiments were performed in a Beckman Optima XL-I, using an AN-50 Ti rotor with 2-channel charcoal-filled centerpieces. Sedimentation velocity experiments were done at 38,000 rpm and 4°C on sample volumes of 400 μL with loading concentrations ranging from 0.020 to 1.300 mg/mL in 25 mM KP_i, pH 6.0, 100 mM KCl, and 10 % (v/v) glycerol (buffer C). Absorbance data were collected at 280 and 230 nm in a continuous mode with a radial step size of 0.005 cm and 10 min time intervals. Sedimentation equilibrium experiments were performed at rotor speeds of 8,000, 10,000, and 12,000 rpm on sample volumes of 100 μL with loading concentrations of 0.020, 0.050, and 0.100 mg/mL OppA in buffer C. The absorbance optics was used to collect data every 0.001 cm with 10 replicates at 280 nm.

Data analysis was done using the XL-I data analysis software (Beckman). The molecular weight of OppA* was determined from the sedimentation equilibrium experiments by global fitting of nine data sets. The partial specific volume ( ) of OppA was 0.7227 mL/mg at 4ºC as calculated from the primary amino acid sequence using SEDNTERP (developed by Hayes, Laue, and Philo, and available at www.jphilo.mailway.com). Values for the solvent density ( ) and viscosity ( ) of the buffer C were determined using the same program and were 1.03878 g/L and 2.2348 $\times 10^{-2}$ Poise, respectively, at 4°C.

Molecular dynamics simulations

Molecular dynamics simulations were performed with a coarse-grain representation of the system using the recently parameterized MARTINI force-field (Marrink *et al*, 2007; Monticelli *et al*, 2008). In the force-field small groups of atoms (usually 4 heavy atoms) are united into a single interacting bead. The force-field was systematically parameterized on the partitioning free energies of many chemical compounds (including the partitioning of amino-acids between polar and apolar phases). The force-field has been shown to represent well the protein structure and function (Periole *et al*, 2007; Treptow *et al*, 2008; Yefimov *et al*, 2008). The protein in the open-state was mapped to its coarse-grain representation from the crystal structure. The octamer peptide (RDMPIQAF) was modeled based on the visible hexamer densities. The simulation box included 15,000 coarse-grain water beads. Simulations were performed using the GROMACS program package (Spoel *et al*, 2005), with the scheme developed for coarse-grain simulations, under periodic boundary conditions. The temperature was weakly coupled (coupling time 0.1 ps) to a thermostat at T = 300K using a Berendsen algorithm (Berendsen *et al*, 1984). The pressure was also weakly coupled at 1 bar (coupling time 1.0 ps, compressibility 5×10^{-6} bar^{-1}) using an isotropic coupling scheme (Berendsen *et al*, 1984). The non-bonded interactions were treated with a switch function from 0.0 to 1.2 nm for the Coulomb interactions and 0.9 to 1.2 nm for the LJ interactions (pair-list update frequency of once per 10 steps). A time step of 25 fs was used. When interpreting the simulation results with the coarse-grain model, a conversion factor of 4 is used, which is the effective speed-up factor in the diffusion dynamics of the coarse-grain water compared to real water (Marrink *et al*, 2007; Monticelli *et al*, 2008). Six simulations with a total simulation time (effective time) of 18 μs were performed.

Miscellaneous

Protein concentrations were determined accordingly (Lowry *et al*, 1951), using bovine serum albumin as a standard. The concentration of purified OppA was determined spectrophotometrically by measuring the absorption at 280 nm and using an extinction coefficient of 1.605 $(mg/mL)^{-1}$ cm^{-1}. Illustrations were produced in PyMol (DeLano, 2002).

Supplementary references

Antonov VK, Alexandrov SL, and Vorotyntseva TI (1976) Reversible association as a possible regulatory mechanism for controlling the activity of the non-specific leucine-binding protein from *Escherichia coli*. *Adv Enzyme Regul* **14**: 269-278

Berendsen HJC, Postma JPM, Vangunsteren WF, Dinola A, and Haak JR (1984) Molecular-dynamics with coupling to an external bath. *J Chem Phys* **81**: 3684-90

Biemans-Oldehinkel E and Poolman B (2003) On the role of the two extracytoplasmic substrate-binding domains in the ABC transporter OpuA. *EMBO J* **22**: 5983-93

DeLano WL (2002) The PyMOL User's Manual.

Gonin S, Arnoux P, Pierru B, Lavergne J, Alonso B, Sabaty M, and Pignol D (2007) Crystal structures of an Extracytoplasmic Solute Receptor from a TRAP transporter in its open and closed forms reveal a helix-swapped dimer requiring a cation for alpha-keto acid binding. *BMC Struct Biol* **7**: 11

Lanfermeijer F, Picon A, Konings W, and Poolman B (1999) Kinetics and consequences of binding of nona- and dodecapeptides to the oligopeptide binding protein (OppA) of *Lactococcus lactis*. *Biochemistry* **38**: 14440-50

Lowry OH, Rosebrough NJ, Farr AL, and Randall RJ (1951) Protein measurement with the Folin phenol reagent. *J Biol Chem* **193**: 265-75

Marrink SJ, Risselada HJ, Yefimov S, Tieleman DP, and de Vries AH (2007) The MARTINI force field: coarse grained model for biomolecular simulations. *J Phys Chem B* **111**: 7812-24

Monticelli L, Kandasamy SK, Periole X, Larson RG, Tieleman DP, and Marrink SJ (2008) The MARTINI coarse-grained force field: Extension to proteins. *J Chem Theory Comput* **4**: 819-34

Periole X, Huber T, Marrink SJ, and Sakmar TP (2007) G protein-coupled receptors self-assemble in dynamics simulations of model bilayers. *J Am Chem Soc* **129**: 10126-32

Quiocho F and Ledvina P (1996) Atomic structure and specificity of bacterial periplasmic receptors for active transport and chemotaxis: variation of common themes. *Mol Microbiol* **20**: 17-25

Rashed I, Shuman H, and Boos W (1976) The dimer of the *Escherichia coli* galactose-binding protein. *Eur J Biochem* **69**: 545-50

Richarme G (1982) Associative properties of the *Escherichia coli* galactose binding protein and maltose binding protein. *Biochem Biophys Res Commun* **105**: 476-81

Richarme G (1983) Associative properties of the *Escherichia coli* galactose-binding protein and maltose-binding protein. *Biochim Biophys Acta* **748**: 99-108

Treptow W, Marrink SJ, and Tarek M (2008) Gating motions in voltage-gated potassium channels revealed by coarse-grained molecular dynamics simulations. *J Phys Chem B* **112**: 3277-82

Yefimov S, van der Giessen E, Onck PR, and Marrink SJ (2008) Mechanosensitive membrane channels in action. *Biophys J* **94**: 2994-3002

der Spoel DV, Lindahl E, Hess B, Groenhof G, Mark A, and Berendsen H (2005) GROMACS: Fast, flexible, and free. *J Comput Chem* **26**: 1701-18

Figure and Table Legends

Figure S1

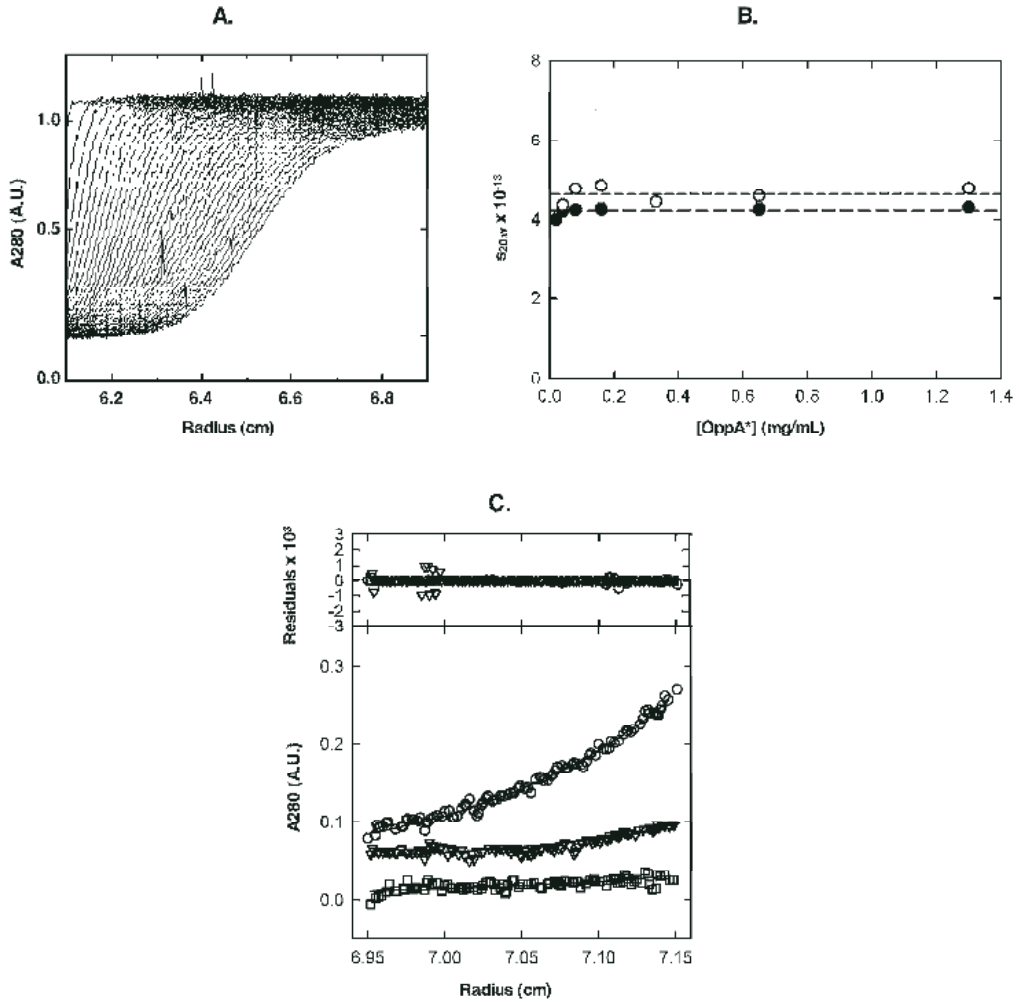

Oligomeric state of OppA*. a) Velocity sedimentation profiles of 0.65 mg/mL OppA*. Time intervals were 10 min. b) Average sedimentation coefficient ($s_{20,w}$) values plotted against the OppA* concentration in the absence (filled circles) or presence (open circles) of a saturating concentration of bradykinin. The horizontal lines indicate the average $s_{20,w}$ values obtained in the absence (long dash) or presence (short dash) of ligand. c) Sedimentation equilibrium analysis. Radial distribution of OppA* at 10,000 rpm and 4ºC with protein loading concentrations of 0.02 (squares), 0.05 (inverted triangles) and 0.10 mg/mL (circles) in the presence of saturating concentrations of bradykinin. The solid lines represent the best fit described by global analysis of nine datasets collected at rotor speeds of 8, 10 and 12 krpm. Residuals are shown in the top graph.

Figure S2

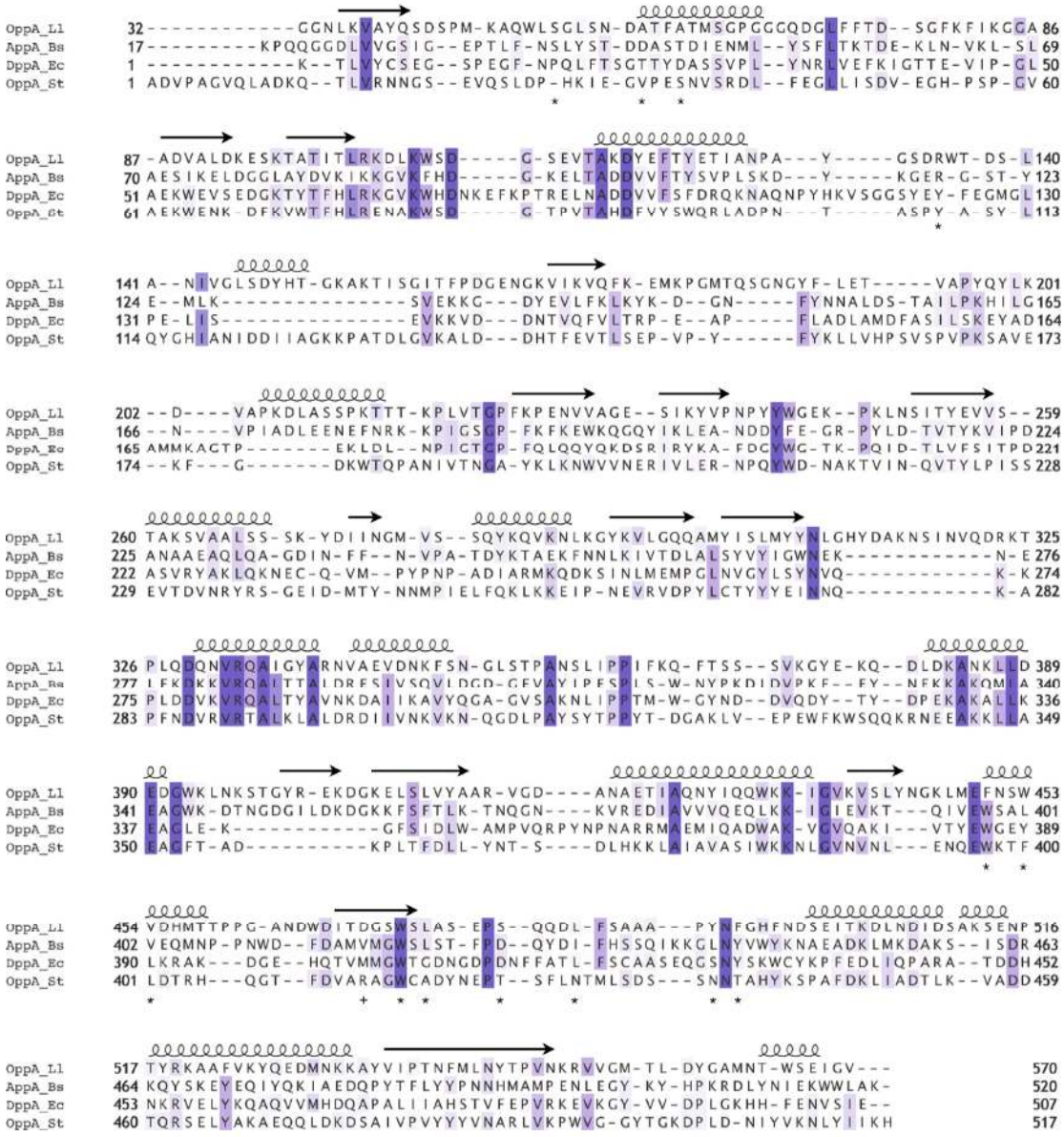

Sequence alignment of OppA of *Lactococcus lactis* (OppA_Ll), AppA of *Bacillus subtilis* (AppA_Bs), DppA of *E. coli* (DppA_Ec) and OppA of *S. typhimurium* (OppA_St), based on an alignment of the 3D structures of the proteins. The percentages of identical residues compared to are: AppA_Bs 20.8%, DppA_Ec 20.5% and OppA_St 20.5%. Arrows above sequence indicate ß-strands, spirals indicate a-helices. Stars below the alignment indicate residues in OppA_Ll that interact with the bound peptide in the closed conformation.

Figure S3

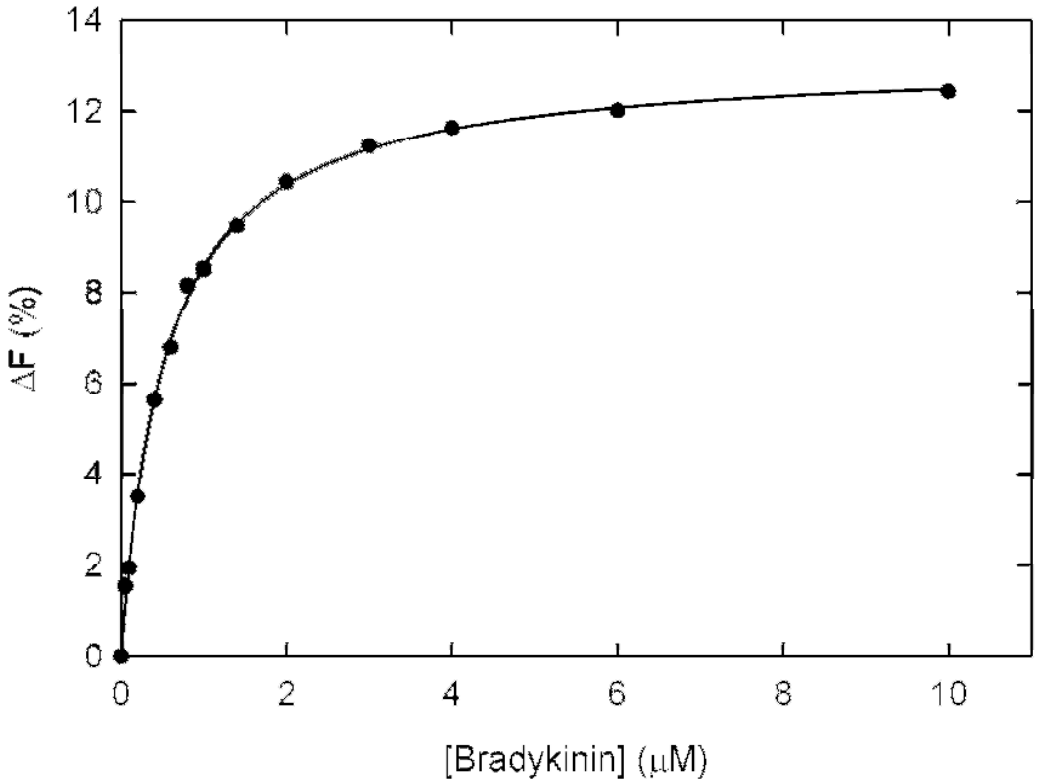

Binding of bradykinin to OppA* monitored by intrinsic protein fluorescence measurements. Titration of OppA* (after GndHCl treatment to remove endogenous peptides) with bradykinin. The protein concentration was 0.5 μM. The change in protein fluorescence (•F) was measured and the data fitted as previously described (Lanfermeijer *et al*, 1999).

Figure S4

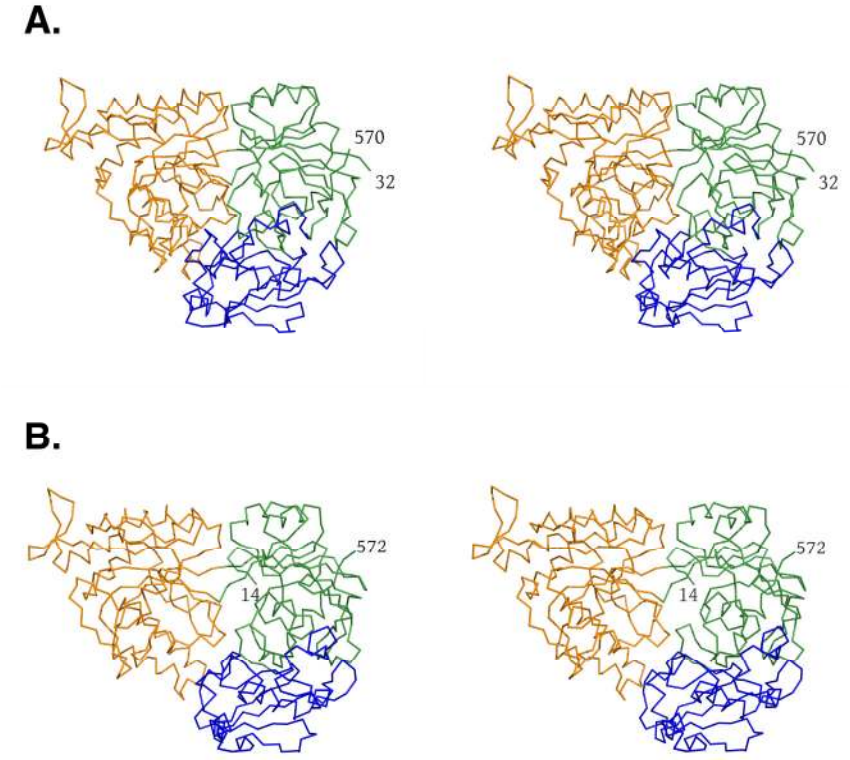

Stereo view of OppA* in the closed (A) and open (B) conformation. The color scheme is the same as in Fig. 2

Figure S5

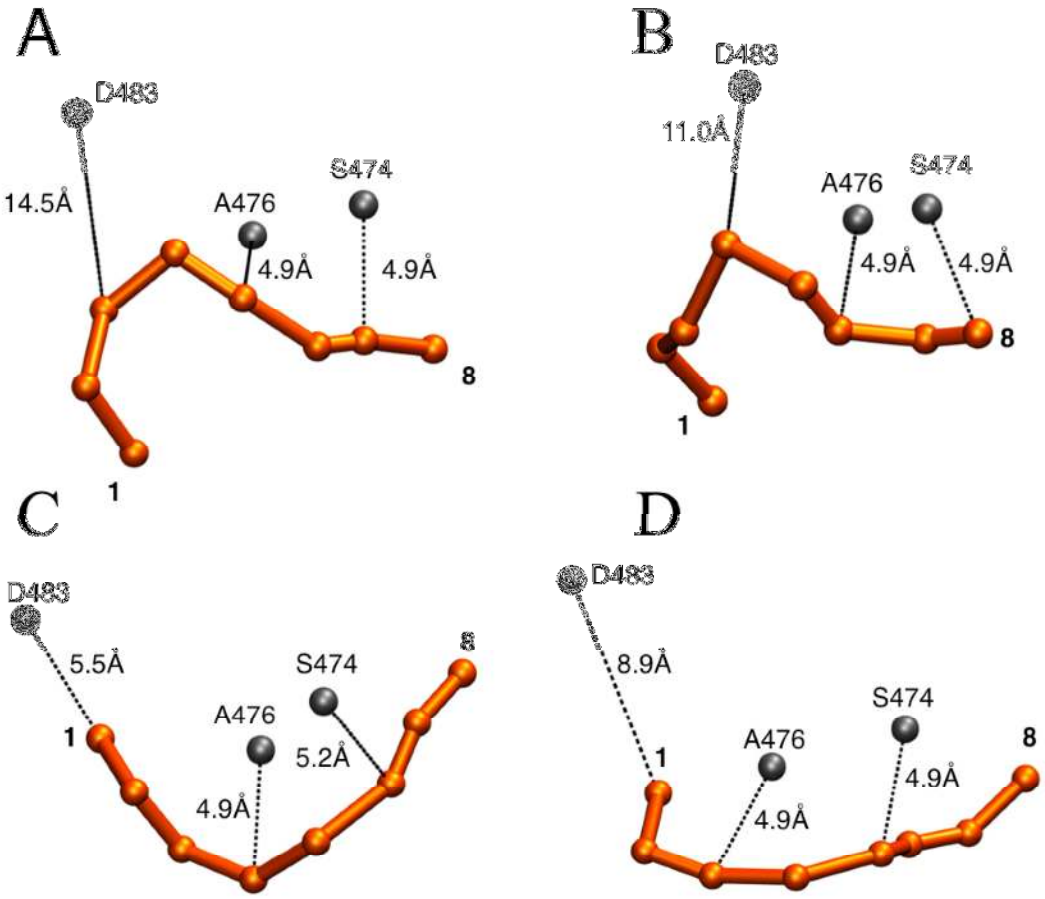

Snapshots of peptide-protein interactions during MD simulation. Panels A-D shows snapshots at different time points during the simulation. Ala476 and Ser474 are at a distance to form hydrogen bonds with different peptide residues in all the snapshots, but Asp483 only in D. The register shift of the peptide at different time points is clearly seen (A=40 ns, B=10 μs, C=11 μs and D= 12.8 μs).

Figure S6

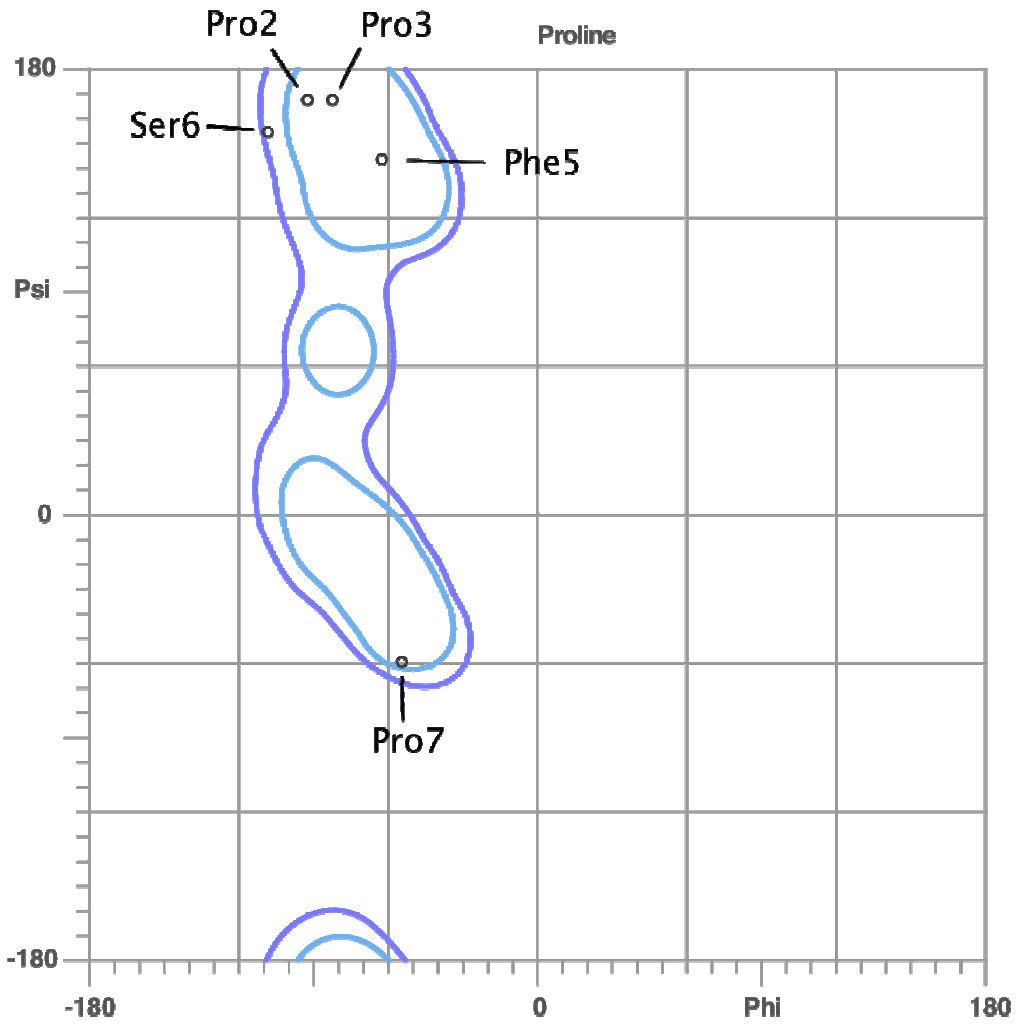

Ramachandran plot of the bound ligand bradykinin (RPPGFSPFR). Ramachandran allowed and favored regions for proline are outlined. Five residues of the bound peptide fit within the limits of proline.

Table I
Data collection and refinement statistics

	Open conformation				Closed conformation					
Data collection										
Ligand	Leu-enkephalin (5 a.a.)	Octapeptide (8 a.a.)	pTH-related peptide (16 a.a.)	Neuropeptid S (20 a.a.)	Bradykinin (9 a.a.)	Endogenous peptide	Endogenous peptide	Endogenous peptide	Endogenous peptide	Endogenous peptide
Space group	$P2_1$	$P2_1$	$P2_1$	$P2_1$	P1	$P2_12_12_1$	$P2_12_12_1$	$P2_12_12_1$	$P2_12_12_1$	$P2_12_12_1$
Cell dimensions										
a, b, c (Å)	40.1, 123.3, 59.7	40.1, 123.3, 59.7	40.1, 123.3, 59.7	40.1, 123.3, 59.7	42.2, 58.6, 61.3	59.1, 74.4, 115.4	59.1, 74.4, 115.4	59.1, 74.4, 115.4	59.1, 74.4, 115.4	59.1, 74.4, 115.4
a, b, g (°)	90, 90, 104	90, 90, 104	90, 90, 104	90, 90, 104	90	90	90	90	90	90
	Native	*Native*	*Native*	*Native*	*Native*	*Native*	*Peak*	*Inflection*	*Remote*	*S-SAD*
Wavelength (Å)	0.934	0.931	0.931	0.931	0.933	1.12	0.9197	0.9200	0.9168	1.7753
Resolution range (Å)	40-1.7	42.3-1.8	37.1-1.5	42.1-1.8	58.2-2.5	30.4-1.3	62.7-2.0	62.3-2.5	62.3-2.5	62.3-2.5
R_{sym}	0.071 (0.392)	0.110 (0.259)	0.043 (0.203)	0.084 (0.257)	0.075 (0.259)	0.070 (0.417)	0.040 (0.077)	0.066 (0.133)	0.045 (0.114)	0.071 (0.163)
I/ **(I)**	10.8 (2.0)	2.3 (2.8)	7.9 (3.2)	3.1 (2.8)	2.0 (2.7)	8.1 (1.8)	13.8 (9.6)	10.7 (4.3)	12.8 (6.2)	7.4 (4.1)
Completeness (%)	99.7 (99.9)	100.0 (100.0)	95.9 (91.8)	97.3 (97.3)	96.2 (95.7)	99.8 (100)	98.1 (97.1)	97.3 (95.9)	98.0 (97.0)	99.5 (98.6)
Redundancy	2.8	3.7	2.4	2.2	2.0	4.6	4.7	4.7	4.7	30.5
Refinement										
Resolution (Å)	35.9-1.7	42.3-1.8	37.1-1.5	42.1-1.8	58.2-2.5	30.4-1.3				
Number of reflections	60836	51692	85971	47251	18131	119254				
R_{work}/R_{free}	0.167/0.205	0.164/0.203	0.165/0.208	0.197/0.248	0.220/0.275	0.133/0.161				
No. atoms										
Protein	4410	4359	4403	4374	4372	4349				
Ligand/ion	30	32	34	34	69	48				
Water	736	763	897	491	138	1111				
B-factors										
Protein	12.7	18.1	12.8	18.9	38.9	9.9				
Ligand/ion	26.1	30.3	29.3	27.2	37.6	13.0				
Water	27.8	32.3	29.9	27.9	31.9	24.6				
R.m.s. deviations										
Bond lengths (Å)	0.011	0.008	0.015	0.007	0.006	0.007				
Bond angles (°)	1.276	1.103	1.562	1.026	1.143	1.269				

*The number in parentheses corresponds to the highest resolution shell

Table II
Identified endogenous peptides. The table lists all identified endogenous peptides with a confidence of >99%, with their corresponding protein.

Peptide	Protein
AEVSGPIPLPTDRS	30S ribosomal protein S10
AEVSGPIPLPTDRSVY	30S ribosomal protein S10
VSGPIPLPTDRS	30S ribosomal protein S10
TNAEVSGPIPLPTDR	30S ribosomal protein S10
AEVESFQLDH	30S ribosomal protein S10
EGISTDPYERKVI	30S ribosomal protein S10
ISTDPYERKVI	30S ribosomal protein S10
TNAEVSGPIPLPTDRS	30S ribosomal protein S10
EVSGPIPLPTDRSVY	30S ribosomal protein S10
TNAEVSGPIPLPTDRSVY	30S ribosomal protein S10
NAEVSGPIPLPTDRSVY	30S ribosomal protein S10
TNAEVSGPIPLPTDRSVYT	30S ribosomal protein S10
GALDTAGVADRKQ	30S ribosomal protein S12
GALDTAGVADRKQS	30S ribosomal protein S12
GADIARAEGYS	30S ribosomal protein S3
GADIARAEGYSEGTVPLHT	30S ribosomal protein S3
IKTQVSGRLN	30S ribosomal protein S3
AVLELAGVADVTSKSLGSNTPINVVR	30S ribosomal protein S5
GADIARAEGYSEG	30S ribosomal protein S5
GADIARAEGYSEGTVPLH	30S ribosomal protein S5
QEVPEAIRKA	30S ribosomal protein S5
SNTPINVVR	30S ribosomal protein S5
SVTAGELREK	50S ribosomal protein L13
ISNGVGVER	50S ribosomal protein L19
NSGINETYTVRK	50S ribosomal protein L19
SGINETYTVRK	50S ribosomal protein L19
TDIPDFRPGDT	50S ribosomal protein L19
EITTSTPEK	50S ribosomal protein L2
GIKVYKPTTN	50S ribosomal protein L2
GIKVYKPTTNG	50S ribosomal protein L2
MTGSDFAEITTSTPEK	50S ribosomal protein L2
MTGSDFAEITTSTPEKS	50S ribosomal protein L2
MTGSDFAEITTSTPEKSL	50S ribosomal protein L2
MTGSDFAEITTSTPEKSLLVS	50S ribosomal protein L2
NMTGSDFAEITTSTPEK	50S ribosomal protein L2
NMTGSDFAEITTSTPEKS	50S ribosomal protein L2
SPMTPWGKPALG	50S ribosomal protein L2
SVMNPNDHPHGGG	50S ribosomal protein L2
SVMNPNDHPHGGGEG	50S ribosomal protein L2
TIEYDPNRTAN	50S ribosomal protein L2
VATIEYDPNRTA	50S ribosomal protein L2
VATIEYDPNRTAN	50S ribosomal protein L2
AIIKTGGKQ	50S ribosomal protein L21
QVKVEEGSVIYVEK	50S ribosomal protein L21
SNYAIIKTGGKQ	50S ribosomal protein L21
AISEGIEVYGINHGYA	6-phosphofructokinase
VELLRDGIGGVAVG	6-phosphofructokinase

AFDVLDEEAGLAQR	Alkyl hydroperoxide reductase subunit C
FDVLDEEAGLAQR	Alkyl hydroperoxide reductase subunit C
DQVDVEDMGGTLR	CTP synthase
AHIDAPGHAD	Elongation factor Tu (EF-Tu)
APGHADYVKN	Elongation factor Tu (EF-Tu)
ASIDAAPEERER	Elongation factor Tu (EF-Tu)
ATDFASIDAAPEER	Elongation factor Tu (EF-Tu)
ATDFASIDAAPEERER	Elongation factor Tu (EF-Tu)
ATDGPMPQTR	Elongation factor Tu (EF-Tu)
DEIERGQVIAKPG	Elongation factor Tu (EF-Tu)
DEIERGQVIAKPGS	Elongation factor Tu (EF-Tu)
DGAILVVAATDGPMPQTR	Elongation factor Tu (EF-Tu)
DIVDEYIPTPER	Elongation factor Tu (EF-Tu)
EGGRTVGSG	Elongation factor Tu (EF-Tu)
EGLAGDNVGALLR	Elongation factor Tu (EF-Tu)
EGLAGDNVGALLRG	Elongation factor Tu (EF-Tu)
FASIDAAPEER	Elongation factor Tu (EF-Tu)
FDNYRPQ	Elongation factor Tu (EF-Tu)
FFDNYRPQ	Elongation factor Tu (EF-Tu)
GIQRDEIERGQ	Elongation factor Tu (EF-Tu)
IDAAPEER	Elongation factor Tu (EF-Tu)
IDAAPEERER	Elongation factor Tu (EF-Tu)
IDAAPEERERG	Elongation factor Tu (EF-Tu)
IEQGTTFSIR	Elongation factor Tu (EF-Tu)
IERGQVIAKPG	Elongation factor Tu (EF-Tu)
IVDEYIPTPER	Elongation factor Tu (EF-Tu)
LAGDNVGALLR	Elongation factor Tu (EF-Tu)
LPVEDVFSITGRG	Elongation factor Tu (EF-Tu)
LTEGLAGDNVGALLR	Elongation factor Tu (EF-Tu)
LTEGLAGDNVGALLRG	Elongation factor Tu (EF-Tu)
SIDAAPEERER	Elongation factor Tu (EF-Tu)
TDFASIDAAPEER	Elongation factor Tu (EF-Tu)
TDFASIDAAPEERER	Elongation factor Tu (EF-Tu)
TDFASIDAAPEERERG	Elongation factor Tu (EF-Tu)
TEGLAGDNVGALLR	Elongation factor Tu (EF-Tu)
TLTEGLAGDNVGAL	Elongation factor Tu (EF-Tu)
TLTEGLAGDNVGALLR	Elongation factor Tu (EF-Tu)
TLTEGLAGDNVGALLRG	Elongation factor Tu (EF-Tu)
TPFFDNYRPQ	Elongation factor Tu (EF-Tu)
VAIEQGTTF	Elongation factor Tu (EF-Tu)
DSNALEQER	GTP-binding protein TypA/BipA homolog
NTAVEYNGTR	GTP-binding protein TypA/BipA homolog
EVFNSFMDEQED	llmg_0152 conserved hypothetical protein
IDGQEEFGKNY	llmg_0152 conserved hypothetical protein
ITIDGQEEFGKNY	llmg_0152 conserved hypothetical protein
LVDENGNESLF	llmg_0152 conserved hypothetical protein
PTEFEEDEQG	llmg_0152 conserved hypothetical protein
VVLQPTEF	llmg_0152 conserved hypothetical protein
VVLQPTEFEEDEQG	llmg_0152 conserved hypothetical protein
GYPETDPHGSEIPTES	llmg_1224 Transcriptional regulator
AEGISTDPYERK	luxS S-ribosylhomocysteinase
AQVTKSKSPAMN	luxS S-ribosylhomocysteinase

EGISTDPYER	luxS S-ribosylhomocysteinase
EGISTDPYERK	luxS S-ribosylhomocysteinase
ILAEGISTDPYER	luxS S-ribosylhomocysteinase
VTAYIPGIGH	luxS S-ribosylhomocysteinase
VTAYIPGIGHN	luxS S-ribosylhomocysteinase
FTLSGEPAEILR	ptsK Hpr kinase/phosphatase
NAPTIVEFSDVEVPQTR	ptsK Hpr kinase/phosphatase
NAPTIVEFSDVEVPQTRIPVK	ptsK Hpr kinase/phosphatase